NEOPLASMA accepted, ahead of print manuscript
Cite article as https://doi.org/10.4149/neo_2026_260507N143

Running title: M2-TAM-derived XCL2 drives PTX resistance in TNBC

M2-TAM-derived XCL2 suppresses paclitaxel sensitivity in triple-negative breast cancer by transcriptionally activating NEK2

Youyuan Deng[1,#], Ye He[1,#], Hongjun Zhao[1], Lifen Ye[1], Jingyong Li[1], Zhiya Hu[2], Huaixiao Zhang[1], Chao Zhang[1], Qishuo Rao[1], Yurong Cai[1], Yiping Xu[1], Jianguo Wang[1,*]

[1]Department of General Surgery, Xiangtan Central Hospital, The Affiliated Hospital of Hunan University, Xiangtan, Hunan, China; [2]Department of Pharmacy, The Third Hospital of Changsha, Changsha, Hunan, China

*Correspondence: wangjianguo@hnu.edu.cn

[#]Contributred equally to this work.

Received May 7, 2026 / Accepted September 15, 2026

Paclitaxel (PTX) resistance is a pivotal factor contributing to the poor prognostic outcome of patients with triple-negative breast cancer (TNBC). M2-type tumor-associated macrophages (M2-TAMs), a key component of the breast tumor microenvironment, foster chemoresistance through the release of multiple cytokines. The chemokine XC motif chemokine ligand 2 (XCL2) is significantly elevated in M2-polarized TAMs, but its role in PTX resistance remains unclear.
Human THP-1 monocytes were first differentiated into M0 macrophages (PMA), followed by M2 polarization with IL-4 and IL-13, with polarization efficiency confirmed by flow cytometry. Cell viability and apoptosis were measured using the CCK-8 assay and flow cytometry, respectively. The binding relationship between transcription factor 4 (TCF4) and the never in mitosis gene A-related kinase 2 (NEK2) promoter was investigated by ChIP and dual-luciferase reporter assays.
Our results showed that M2-TAM-secreted XCL2 reduced PTX-induced apoptosis and enhanced TNBC cell viability. Mechanistically, XCL2 was associated with XCR1 activation and subsequent β-catenin nuclear translocation, which may enable TCF4 to transcriptionally upregulate NEK2. As expected, TCF4 knockdown in TNBC cells reduced PTX resistance, while this effect was reversed by NEK2 overexpression. In addition, NEK2 knockdown in TNBC cells reversed the promoting effect of M2-CM on PTX resistance in TNBC. *In vivo*, M2-TAMs were associated with accelerated tumor growth under PTX treatment, whereas XCL2 knockdown restored PTX efficacy.
To conclude, M2-TAM-derived XCL2 enhanced PTX resistance in TNBC cells by activating the β-catenin/TCF4/NEK2 pathway. Targeting this signaling may provide novel strategies to overcome PTX resistance in TNBC.

Key words: triple-negative breast cancer; M2-type tumor-associated macrophages; PTX resistance; XCL2; XCR1; β-catenin/TCF4; NEK2

Accepted manuscript

Breast cancer ranks as the most prevalent malignant neoplasm in females, making up 25% of all cancer cases [1]. Triple-negative breast cancer (TNBC) distinguished by its lack of estrogen receptor, progesterone receptor, and HER2 expression, represents the most aggressive breast cancer subtype [2]. Chemotherapy is the standard treatment for TNBC [3]. Paclitaxel (PTX)-based chemotherapy is a first-line regimen for TNBC. Despite advances in chemotherapy, the development of resistance remains a major contributor to TNBC relapse and poor prognosis [4]. Emerging evidence highlights the critical role of the tumor immune microenvironment (TME) in driving chemoresistance in TNBC [5]. TME harbors abundant tumor-associated macrophages (TAMs), most of which exhibit a pro-tumor M2 phenotype, secreting immunosuppressive cytokines and recruiting immunosuppressive cells, thereby contributing to chemotherapy resistance [6]. Therefore, M2-polarized macrophages in tumor tissues present a viable strategy for overcoming chemoresistance in TNBC.

The XC motif chemokine ligand 2 (XCL2), a bifunctional chemokine belonging to the XC subfamily, is constitutively produced by thymic medullary epithelial cells under steady-state conditions and by activated T cells, natural killer (NK) cells, and natural killer T cells (NKT) cells during infection or inflammatory responses; it exerts its effects by binding to its exclusive receptor, X-C motif chemokine receptor 1 (XCR1) [7]. Our previous study identified XCL2 as a potential mediator of chemoresistance in breast cancer [8]. In addition, XCL2 is highly expressed in macrophages and correlates with M2-TAM infiltration in breast cancer [9]. Notably, XCR1 silencing inhibited malignant behaviors of breast cancer cells and blocked XCL1-induced nuclear translocation of β-catenin [10]. As an extensively characterized protein, β-catenin executes its nuclear roles primarily through association with the transcription Factor 7-Like 2 (TCF4, also known as TCF7L2, Gene ID: 6934) [11]. Activation of β-catenin/TCF4 signaling diminishes PTX sensitivity in breast cancer cells [12]. Nevertheless, whether M2-TAMs contribute to PTX resistance in TNBC cells by regulating XCR1-mediated β-catenin/TCF4 signaling through the release of XCL2 remains unexplored.

Never in mitosis gene A-related kinase 2 (NEK2) kinase is a critical regulator of mitotic processes, and its dysregulation drives chromosomal instability and aneuploidy hallmarks of many solid

Accepted manuscript

tumors, including TNBC [13]. It has been widely reported that NEK2 upregulation promotes malignant behaviors of TNBC cells [14, 15]. Importantly, NEK2 silencing restored PTX sensitivity in TNBC cells [16, 17]. Given that our analysis identified TCF4 binding sites within the NEK2 promoter, we propose that β-catenin/TCF4-mediated transcriptional activation of NEK2 represents a potential mechanism underlying PTX resistance in TNBC.

Based on the above evidence, we hypothesize that M2-TAM-secreted XCL2 may activate XCR1-mediated β-catenin/TCF4 signaling in TNBC cells, potentially leading to transcriptional upregulation of NEK2 and subsequent PTX resistance. Our study may pave the way for developing combination therapies targeting M2-TAMs or downstream effectors to overcome PTX resistance in TNBC.

Materials and Methods

Reagents and antibodies. Primary antibodies used for Western blot and immunohistochemistry were as follows: anti-XCL2 (rabbit polyclonal, Antibodies-online, Aachen, Germany, #ABIN7636554, 1:1000 for Western blot; 1:50 for immunohistochemistry), anti-XCR1 (rabbit polyclonal, Invitrogen, CA, USA, #PA5-116133, 1:1000 for Western blot), anti-TCF4 (rabbit monoclonal, Abcam, Cambridge, UK, #ab217668, 1:10000 for Western blot; 1:100 for ChIP), anti-NEK2 (rabbit polyclonal, Proteintech, Hubei, China, #24171-1-AP, 1:1000 for Western blot; 1:100 for immunohistochemistry), anti-β-catenin (mouse monoclonal, Invitrogen, #13-8400, 1:1000 for Western blot), anti-Bax (rabbit monoclonal, Abcam, #ab32503, 1:1000 for Western blot; 1:250 for immunohistochemistry), anti-cleaved caspase-3 (rabbit polyclonal, Abcam, #ab32042, 1:1000 for Western blot), anti-Ki67 (rabbit monoclonal, Abcam, #ab16667, 1:200 for immunohistochemistry), anti-GAPDH (mouse monoclonal, Abcam, #ab8245, 1:5000 for Western blot), isotype-matched IgG (rabbit monoclonal, Abcam, #ab172730, 1:100 for immunohistochemistry), and anti-IgG (rabbit monoclonal, Abcam, #ab172730, 1:50 for ChIP). Secondary antibodies for Western blot: HRP-conjugated goat anti-rabbit IgG (Abcam, #ab7090, 1:10000) and HRP-conjugated goat anti-mouse IgG (Abcam, #ab205719, 1:10000). Secondary antibody for immunohistochemistry: HRP-linked goat anti-rabbit IgG (Invitrogen, #31460, 1:500). Key reagents: RPMI-1640 medium (Gibco, MD, USA, #11875093); FBS (Gibco, #10099141C);

Accepted manuscript

104 Penicillin-streptomycin (Gibco, #15140122), DMEM (Gibco, #11965092), DMEM/F12 medium
105 (Gibco, #11330032), Horse serum (Gibco, #26050088), Epidermal growth factor (PeproTech, NJ,
106 USA, #100-15), Hydrocortisone (Sigma-Aldrich, MO, USA, #H0888), Cholera toxin
107 (Sigma-Aldrich, #C8052), Insulin (Sigma-Aldrich, #I9278), Opti-MEM™ I Reduced Serum
108 Medium (Gibco, #31985062), Phenylmethylsulfonyl fluoride (PMSF; Beyotime, Shanghai, China,
109 #ST506), Protease inhibitor cocktail (Beyotime, #P1005), BCA Protein Assay Kit (Beyotime,
110 #P0012), TRIzol Reagent (Invitrogen, #15596026), PrimeScript RT Kit (Takara, Osaka, Japan,
111 #RR047A), SYBR Green qPCR Master Mix (Roche, Basel, Switzerland, #04913914001), PARIS™
112 Kit for nuclear/cytoplasmic fractionation (Invitrogen, #AM1921), RIPA lysis buffer (Beyotime,
113 #P0013B), ECL substrate (Millipore, MA, USA, #WBKLS0500), PVDF membranes (Millipore,
114 #IPVH00010), ChIP assay kit (Cell Signaling Technology, MA, USA, #9003), Lipofectamine™
115 3000 (Invitrogen, #L3000015), Dual Luciferase Assay Kit (Promega, WI, USA, #E1910), CCK-8
116 reagent (Beyotime, #C0038), Annexin V-FITC/PI Apoptosis Detection Kit (Beyotime, #C1062),
117 Human XCL2 ELISA Kit (Raybiotech, Guangdong, China, #ELH-XCL2-1), Fc receptor blocking
118 solution (BioLegend, CA, USA, #422302), CD206-PE antibody (mouse anti-human, BioLegend,
119 #321105), CD163-PE antibody (mouse anti-human, BioLegend, #326505), phorbol 12-myristate
120 13-acetate (PMA; Sigma-Aldrich, #P8139), recombinant human IL-4 (PeproTech, #200-04),
121 recombinant human IL-13 (PeproTech, #200-13), Polybrene (Sigma-Aldrich, #TR-1003-G), DAB
122 substrate (ZSGB-BIO, Beijing, China, #ZLI-9018), Hematoxylin (Sigma-Aldrich, #H9627),
123 Matrigel (Corning, NY, USA, #356234), Bovine serum albumin (Sigma-Aldrich, #A2153),
124 Puromycin (Sigma-Aldrich, #P8833), Neutral balsam (Sinopharm, #10004160), Dimethyl sulfoxide
125 (DMSO; Sigma-Aldrich, #D2650), and paclitaxel (PTX; Sigma-Aldrich, #T7402).
126 **Cell culture and treatment.** Human TNBC cell lines MDA-MB-468 and MDA-MB-231, human
127 mammary epithelial cell line MCF-10A, human monocytic cell line THP-1, and human embryonic
128 kidney cell line 293T were obtained from the American Type Culture Collection (ATCC, VA, USA).
129 THP-1 cells were maintained in RPMI-1640 medium supplemented with 10% FBS and 1%
130 penicillin-streptomycin at 37 °C with 5% CO_2, whereas the breast cancer lines were propagated in
131 DMEM with 10% FBS and 1% penicillin-streptomycin. MCF-10A cells were maintained in
132 DMEM/F12 medium supplemented with 5% horse serum, 20 ng/ml epidermal growth factor, 0.5

Accepted manuscript

133 μg/ml hydrocortisone, 100 ng/ml cholera toxin, 10 μg/ml insulin, and 1% penicillin-streptomycin.
134 To generate M2-polarized macrophages, THP-1 cells were first differentiated into M0 macrophages
135 using 100 ng/ml PMA for 24 h. Adherent cells were subsequently stimulated with 20 ng/ml each of
136 recombinant human IL-4 and IL-13 for an additional 24 h to induce the M2 phenotype. To prepare
137 conditioned medium (CM), macrophages were washed three times with PBS and incubated in fresh
138 serum-free RPMI-1640 for 24 h. The supernatant was collected, centrifuged at 300 × g for 5 min at
139 4 °C to remove cell debris, filtered through a 0.22 μm sterile filter (Millipore, #SLGV033RS), and
140 stored at -80 °C. Before application to TNBC cells, CM was thawed at 37 °C and mixed 1:1 with
141 complete DMEM. MDA-MB-468 and MDA-MB-231 cells were cultured in M2-CM for 6 h as
142 previously described [6]. For PTX treatment, breast cells were treated with PTX at concentrations
143 ranging from 0 to 50 nM for 72 h as previously reported [18].
144 **Cell transfection.** The small interfering RNA (si-XCL2, si-XCR1, si-β-catenin, si-TCF4, and
145 si-NEK2), overexpression plasmids (oe-NEK2), and their negative controls (si-NC and oe-vector)
146 were purchased from Genepharma (Shanghai, China). For transfection, TNBC cells were seeded at
147 1.5×10^5 cells/well in 6-well plates and cultured overnight to reach 70-80% confluence.
148 Transfection was performed using Lipofectamine™ 3000 according to the manufacturer's protocol.
149 Briefly, 5 μl Lipofectamine™ 3000 reagent and 2.5 μg siRNA or 2.5 μg plasmid DNA were diluted
150 separately in 125 μl Opti-MEM™ I Reduced Serum Medium, incubated at room temperature for 5
151 min, mixed together, and incubated for an additional 15 min. The complexes were then added
152 dropwise to the cells and cells were harvested 48 hours post-transfection for further analysis.
153 **Reverse transcription quantitative polymerase chain reaction (RT-qPCR).** Total RNA was
154 extracted from tissues or cells using TRIzol. RNA concentration and purity were assessed using a
155 NanoDrop 2000 spectrophotometer (ThermoFisher Scientific, MA, USA), with A260/A280 ratios
156 between 1.8 and 2.0 considered acceptable. First-strand cDNA was synthesized from 1 μg total
157 RNA using the PrimeScript RT Kit. Quantitative PCR was performed using SYBR Green qPCR
158 Master Mix on a QuantStudio 5 Real-Time PCR System (Applied Biosystems, CA, USA) in a 20 μl
159 reaction volume containing 10 μl SYBR Green Master Mix, 0.8 μl each of forward and reverse
160 primers (10 μM), 2 μl cDNA template, and 6.4 μl nuclease-free water. The thermal cycling
161 conditions were: initial denaturation at 95 °C for 10 min, followed by 40 cycles of 95 °C for 15 s

Accepted manuscript

162 and 60 °C for 1 min. A melting curve analysis was performed to confirm specific amplification.
163 Relative gene expression was normalized to β-actin using the $2^{-\Delta\Delta CT}$ method. The primers used in
164 the study were listed as follows (5'-3'): TCF4 (F): CTCCAAAGAAGTGTCGGGCA, TCF4 (R):
165 TCAGTCTGTGACTTGGCGTC; NEK2 (F): TGCTTCGTGAACTGAAACATCC, NEK2 (R):
166 CCAGAGTCAACTGAGTCATCACT; XCL2 (F): GTGTAGGGAGTGAAGTCTCACATAG,
167 XCL2 (R): CCACGTGGCTTGTGGATCA; XCR1 (F): GCTGGGGTCCCTACAACTTC, XCR1
168 (R): GTTTCAGGTGTGTGCGGAAC; β-actin (F): CCCTGGAGAAGAGCTACGAG, β-actin (R):
169 CGTACAGGTCTTTGCGGATG.
170 **Western blot.** Nuclear and cytoplasmic proteins were isolated from cells using the PARIS™ Kit.
171 Protein samples were extracted from tissues or cells using RIPA lysis buffer supplemented with 1%
172 phenylmethylsulphonyl fluoride and 1% protease inhibitor cocktail. Lysates were incubated on ice
173 for 30 min with vortexing every 10 min, then centrifuged at 12,000 × g for 15 min at 4 °C.
174 Supernatant protein concentrations were determined using the BCA Protein Assay Kit. Equal
175 amounts of protein (30 μg/lane) were separated by 10% SDS-PAGE, followed by transfer onto
176 PVDF membranes. Membranes were blocked with 5% non-fat milk for 1 h and incubated overnight
177 at 4 °C with primary antibodies against TCF4, NEK2, XCL2, XCR1, Bax, cleaved caspase 3,
178 β-catenin, and GAPDH. Following 10 min TBST washes, membranes were incubated with
179 HRP-conjugated secondary antibodies for 1 h at room temperature. Immunoreactive bands were
180 detected using the ECL kit.
181 **Enzyme-linked immunosorbent assay (ELISA).** The secretion level of XCL2 in cell culture
182 supernatants was quantified using the Human XCL2 ELISA Kit according to the manufacturer's
183 instructions. This sandwich ELISA kit uses recombinant human XCL2 as the standard protein for
184 calibration, with a detection range of 0.52-480 ng/ml and a sensitivity of 0.52 ng/ml. Cell culture
185 supernatants were collected and centrifuged at 300 × g for 5 min at 4 °C to remove debris.
186 Preliminary experiments indicated that XCL2 concentrations in M2-conditioned medium exceeded
187 the upper limit of the standard curve (480 ng/ml). Therefore, samples were diluted 2-fold with the
188 manufacturer-provided sample diluent prior to loading, ensuring that all measurements fell within
189 the validated linear range of the assay. Standards and samples (100 μl/well) were loaded in triplicate
190 onto pre-coated 96-well plates and incubated for 2.5 h at room temperature with gentle shaking.

Accepted manuscript

191 Wells were washed four times with 300 μl wash buffer per well. Biotinylated detection antibody
192 (100 μl/well) was added and incubated for 1 h at room temperature. After washing,
193 streptavidin-conjugated HRP (100 μl/well) was added and incubated for 45 min at room
194 temperature. Following another four washes, TMB one-step substrate reagent (100 μl/well) was
195 added and incubated for 30 min at room temperature in the dark. The reaction was terminated by
196 adding 50 μl stop solution (2 M sulfuric acid) per well. Absorbance at 450 nm was measured
197 immediately using a SpectraMax i3x microplate reader (Molecular Devices, CA, USA). A standard
198 curve was constructed using a four-parameter logistic regression, and sample concentrations were
199 calculated from the curve. The final concentrations were obtained by multiplying the measured
200 values by the dilution factor of 2. All measurements were performed in triplicate for each sample,
201 with intra-assay coefficient of variation (CV) < 10% and inter-assay CV < 15%.
202 **Flow cytometry analysis of M2 macrophage polarization markers.** Cultured macrophages were
203 harvested using a cell scraper, washed twice with cold PBS, and resuspended in FACS buffer (PBS
204 with 2% FBS and 0.1% sodium azide) at a concentration of 1×10^6 cells/ml. Cells were incubated
205 with Fc receptor blocking solution for 10 min at 4 °C to minimize non-specific binding. Cells were
206 stained with CD206-PE or CD163-PE for 30 min at 4 °C in the dark. After two washes with cold
207 FACS buffer, cells were resuspended in 300 μl FACS buffer and analyzed using a Beckman
208 CytoFLEX flow cytometer (Beckman Coulter, CA, USA). Data were analyzed using CytExpert
209 software (version 2.4, Beckman Coulter). At least 10,000 events were acquired per sample.
210 **Flow cytometry analysis of apoptosis.** Apoptosis was assessed by Annexin V-FITC/PI staining.
211 Briefly, cells were harvested, washed twice with cold PBS, and resuspended in 1× Annexin V
212 Binding Buffer at a concentration of 1×10^6 cells/ml. Cells (100 μl, 1×10^5 cells) were transferred
213 to a new tube and stained with 5 μl Annexin V-FITC and 5 μl propidium iodide (PI, 50 μg/ml) for
214 15 min at room temperature in the dark. After incubation, 400 μl binding buffer was added, and
215 samples were immediately analyzed using a Beckman CytoFLEX flow cytometer. Data were
216 analyzed using CytExpert software. Early apoptotic cells (Annexin V^+/PI^-) and late
217 apoptotic/necrotic cells (Annexin V^+/PI^+) were quantified. At least 10,000 events were acquired
218 per sample.
219 **Chromatin immunoprecipitation (ChIP) assay.** ChIP assays were performed using the

Accepted manuscript

220 SimpleChIP® Enzymatic Chromatin IP Kit. Cells (1×10^7 per sample) were crosslinked with 1%
221 formaldehyde for 10 min at room temperature with gentle rotation. Crosslinking was quenched by
222 adding 125 mM glycine for 5 min at room temperature. Cells were washed twice with cold PBS,
223 scraped into 1 ml PBS with 1% PMSF, and pelleted by centrifugation at 1,000 × g for 5 min at 4 °C.
224 Cell pellets were resuspended in 500 µl buffer A and incubated on ice for 10 min. Nuclei were
225 collected by centrifugation at 3,000 × g for 5 min at 4 °C, resuspended in 500 µl buffer B, and
226 digested with micrococcal nuclease for 20 min at 37 °C with frequent mixing. Digestion was
227 stopped by adding 50 µl 0.5 M EDTA. Nuclear membranes were disrupted by sonication using a
228 Bioruptor® Pico sonication device (Diagenode, Belgium) with three 10 second pulses at high
229 intensity, 30 second rest intervals on ice. Lysates were centrifuged at 10,000 × g for 10 min at 4 °C,
230 and supernatants (containing chromatin fragments of 200-500 bp) were collected. For
231 immunoprecipitation, 50 µl protein G magnetic beads were washed twice with buffer B and
232 incubated with 5 µg anti-TCF4 antibody or 5 µg anti-IgG control antibody for 2 h at 4 °C with
233 rotation. Beads were washed twice with buffer B, then incubated with 100 µl chromatin lysate
234 overnight at 4 °C with rotation. After incubation, beads were washed, and bound DNA was eluted,
235 reversed crosslinked, and purified. The enrichment of TCF4 at the NEK2 promoter was assessed by
236 qPCR using specific primers targeting predicted binding sites. The relative enrichment of TCF4 at
237 each binding site was calculated as a percentage of input DNA.
238 **Dual-luciferase reporter assay.** The wild-type (wt) and mutant (mut) binding sites of TCF4 in the
239 NEK2 promoter were synthesized and cloned into the psicheck2 vector (Promega, WI, USA). The
240 wt construct contained intact putative TCF4-binding sites with the sequence AGTGCAAAG (Site 1)
241 and GGTTAAAAG (Site 2), whereas mut1 lacked Site 1 (ΔAGTGCAAAG) and mut2 lacked Site 2
242 (ΔGGTTAAAAG). Cells were co-transfected with NEK2 wt or NEK2 mut1/2 plasmids and
243 oe-vector or oe-TCF4 by Lipofectamine™ 3000. The luciferase activities were determined by the
244 Dual Luciferase Assay kit.
245 **Cell counting kit-8 (CCK-8) assay.** TNBC cells were seeded at 5×10^3 cells/well in 96-well plates
246 in 100 µl complete medium and cultured overnight. After treatments, 10 µl CCK-8 reagent was
247 added to each well, and plates were incubated for 2 h at 37 °C in a humidified atmosphere with 5%
248 CO_2. Absorbance at 450 nm was measured using a Multiskan FC microplate reader (ThermoFisher

Accepted manuscript

249 Scientific).

250 **Animal experiments.** Female Balb/c nude mice (4 weeks old) were sourced from Charles River
251 (Beijing, China). Animals were housed in a specific pathogen-free (SPF) facility with controlled
252 temperature (22±2 °C), humidity (50-60%), and a 12 h light/dark cycle. Following a 7-day
253 acclimation period with standard rodent chow and water ad libitum, animals were randomly
254 assigned to five cohorts (n=6): MDA-MB-468, MDA-MB-468+PTX, MDA-MB-468+M2+PTX,
255 MDA-MB-468+M2+sh-NC+PTX, and MDA-MB-468+M2+sh-XCL2+PTX. THP-1 monocytes
256 were transduced with lentiviral particles encoding either scramble shRNA (sh-NC) or
257 XCL2-targeting shRNA (sh-XCL2) to generate stable knockdown lines. In brief, THP-1 cells were
258 seeded at 2×10^5 cells/well in 6-well plates and transduced with lentiviral particles at a
259 multiplicity of infection (MOI) of 20 in the presence of 8 μg/ml polybrene for 24 h. After
260 transduction, cells were washed and cultured in complete RPMI-1640 for 48 h, followed by
261 selection with 2 μg/ml puromycin for 14 days. Surviving colonies were pooled and expanded.
262 Knockdown efficiency was verified by Western blot and RT-qPCR before use in subsequent
263 experiments. The resulting populations were polarized to M2 macrophages. The generated M2,
264 sh-NC-M2, and sh-XCL2-M2 macrophages (9×10^5 cells in 50 μl) were mixed with MDA-MB-468
265 cells (3×10^5 cells in 50 μl) in a 1:1 mixture of Matrigel and PBS. The cell suspension (100 μl total
266 volume) was injected into the fourth inguinal mammary fat pad of each mouse using a 26-gauge
267 needle. PTX was dissolved in saline containing 1% dimethyl sulfoxide and administered
268 intraperitoneally at a dose of 10 mg/kg every 3 days starting at day 7 post-inoculation (treatment
269 days: 7, 10, 13, 16, 19). Vehicle control (saline with 1% DMSO) was administered to non-PTX
270 groups on the same schedule. Tumor growth was monitored every 3 days starting from day 7
271 post-inoculation by measuring tumor length (L) and width (W) with digital calipers, and tumor
272 volume was calculated using the formula: $V=(L \times W^2)/2$. Specific humane endpoints included: i)
273 tumor volume exceeding 2,000 mm^3; ii) tumor ulceration or necrosis; iii) body weight loss
274 exceeding 20% of initial weight; iv) signs of severe pain or distress (hunching, reduced mobility, or
275 inability to access food/water). The endpoint was set at day 22 based on the following
276 considerations: i) Treatment schedule: the 22-day endpoint allowed for five complete PTX
277 treatment cycles (every 3 days from day 7), ensuring sufficient time for therapeutic response

Accepted manuscript

assessment, consistent with established TNBC xenograft protocols using the same dosing regimen [19]; ii) Animal welfare considerations: day 22 was selected to balance statistical power with humane endpoints, minimizing animal suffering while ensuring adequate duration for treatment efficacy evaluation, comparable to similar studies investigating TAM-mediated chemoresistance in breast cancer xenografts [19, 20]. At the study endpoint (day 22), mice were euthanized, and excised tumors were collected.

Ethics approval and consent to participate. All procedures adhered to the Hubei Provincial Center for Disease Control and Prevention Laboratory Animal Care and Use Committee (Approval No. 202510502).

Immunohistochemistry. Paraffin-embedded tumor sections (4 μm) were deparaffinized in xylene for 15 min (three changes), rehydrated through graded ethanol series (100%, 95%, 85%, 75%, each for 5 min), and rinsed in distilled water. Heat-induced antigen retrieval was performed in 10 mM sodium citrate buffer (pH 6.0) at 100 °C for 20 min in a microwave oven (medium power). Endogenous peroxidases were blocked with 3% hydrogen peroxide, and non-specific binding sites were saturated using 5% bovine serum albumin for 60 min. Primary antibodies against XCL2, Bax, NEK2, and Ki67 were applied overnight at 4 °C. After TBST washes, HRP-linked secondary antibody was applied for 1 h at room temperature. Color development was performed using DAB substrate for 3-5 min under microscopic monitoring. Sections were counterstained with hematoxylin for 30 s, dehydrated through graded ethanol, cleared in xylene, and mounted with neutral balsam. Digital images were acquired using a Nikon microscope (Tokyo, Japan). For negative controls, isotype-matched IgG was used instead of primary antibodies. all antibodies used were commercially validated by the manufacturers, and all procedures strictly followed the manufacturers' protocols. For quantification, the percentage of positive cells were evaluated independently by two blinded investigators. Five random fields per section were analyzed.

Statistical analysis. Data were analyzed using GraphPad Prism 9.0 (GraphPad Software, CA, USA) and are presented as mean±standard deviation (SD). For *in vitro* experiments, n=3 indicates three independent biological replicates performed on separate days with independently prepared cells and reagents. For *in vivo* studies, n=6 represents six animals per group. Normality of data distribution was assessed using the Shapiro-Wilk test, and homogeneity of variance was confirmed using

Accepted manuscript

307 Levene's test before applying parametric tests. Comparisons between two groups were performed
308 using Student's t-test (two-tailed). For multiple group comparisons, one-way analysis of variance
309 (ANOVA) followed by Tukey's post hoc test was applied, two-way ANOVA followed by Sidak's
310 post hoc test was used to compare group differences at each time point. A p-value < 0.05 was
311 considered statistically significant.
312
313 **Results**
314 **M2-TAMs inhibited the sensitivity of TNBC cells to PTX by secreting XCL2.** To investigate
315 how macrophage polarization modulates PTX sensitivity in TNBC, we first established M2
316 macrophage by differentiating THP-1 monocytes with PMA (M0) followed by IL-4/IL-13
317 stimulation (M2). Flow cytometry confirmed successful M2 polarization based on elevated
318 expression of CD206 and CD163 (Figure 1A). Importantly, we found that M2 macrophages
319 exhibited significantly higher XCL2 expression compared to M0 controls (Figures 1B, 1C), which
320 was further validated by increased XCL2 secretion in M2-CM (Figure 1D). To functionally
321 interrogate XCL2's role, we generated XCL2-knockdown M2-TAMs by transfecting si-XCL2 into
322 cells. As shown in Figures 1E and 1F, si-XCL2 transfection significantly reduced XCL2 expression
323 in cells. ELISA analysis also confirmed that M2+si-XCL2-CM contained significantly reduced
324 XCL2 compared to control M2-CM (Figure 1G). We next assessed whether M2-derived XCL2
325 affected the sensitivity of TNBC cells to PTX. CCK-8 assay M2-CM treatment substantially
326 reduced PTX sensitivity in MDA-MB-468 and MDA-MB-231 cells across PTX dose range (0-50
327 nM), while M2+si-XCL2-CM lost the ability to promote PTX resistance compared to M2-CM
328 (Figure 1H). Further experiments revealed that while PTX monotherapy significantly reduced
329 TNBC cell viability, concomitant M2-CM treatment rescued cell survival, but M2+si-XCL2-CM
330 lost its promoting effect on the survival of TNBC cells compared with M2-CM (Figure 1I).
331 Moreover, PTX treatment induced apoptosis in TNBC cells, and M2-CM treatment attenuated
332 PTX-induced apoptosis, whereas M2+si-XCL2-CM lost this anti-apoptotic effect compared with
333 M2-CM (Figure 1J). Consistently, PTX upregulated pro-apoptotic Bax and cleaved caspase-3 in
334 TNBC cells, but these effects were partially counteracted by M2-CM (Figure 1K). Again,
335 M2+si-XCL2-CM lost the ability to modulate these apoptotic markers (Figure 1K). Together,

Accepted manuscript

336 M2-TAMs reduced the sensitivity of TNBC cells to PTX through XCL2 secretion.

337 **M2-TAM-derived XCL2 was associated with reduced PTX sensitivity in TNBC cells via the**
338 **XCR1/β-catenin axis.** As previously reported, XCR1 (the exclusive receptor of XCL2) knockdown
339 inhibited the progression of breast cancer by blocking XCL1-mediated β-catenin nuclear
340 translocation [10]. As shown in Figure 2A, PTX treatment significantly reduced nuclear β-catenin
341 accumulation in MDA-MB-468 and MDA-MB-231 cells, and M2-CM restored its nuclear
342 localization, while M2+si-XCL2-CM lost this ability. We subsequently silenced XCR1 in
343 MDA-MB-468 and MDA-MB-231 cells, and si-XCR1 transfection significantly reduced XCR1
344 expression and β-catenin nuclear localization in TNBC cells (Figures 2B, 2C). We next assessed the
345 functional consequences of the XCR1/β-catenin axis. It was observed that M2-CM treatment
346 prevented PTX-induced decrease in TNBC cell viability, whereas XCR1 knockdown reversed this
347 effect of M2-CM (Figure 2D). In addition, M2-CM treatment suppressed PTX-induced apoptosis in
348 TNBC cells, while XCR1 silencing reversed this effect (Figure 2E). Consistently, M2-CM
349 downregulated Bax and cleaved caspase-3 protein levels in PTX-treated TNBC cells, while XCR1
350 silencing abrogated this effect (Figure 2F). Collectively, M2-TAM-derived XCL2 was associated
351 with inhibited PTX-driven apoptosis and promoted PTX resistance in TNBC, potentially acting
352 through the XCR1/β-catenin axis.

353 **β-catenin/TCF4 transcriptionally activated NEK2 expression in TNBC cells.** NEK2 is an
354 oncogene implicated in chemoresistance during TNBC development [16]. In the current research,
355 bioinformatics analysis using the JASPAR database predicted three potential TCF4-binding motifs
356 (AGATCAAGG, AGTGCAAAG, GGTTAAAAG) within the NEK2 promoter region (Figure 3A).
357 ChIP-qPCR assay demonstrated that TCF4 significantly enriched the promoter region including
358 AGTGCAAAG and GGTTAAAAG, but not the distal AGATCAAGG site (Figure 3B), indicating
359 that TCF4 preferentially binds at two proximal motifs. We also performed dual-luciferase reporter
360 assays in 293T cells using wt NEK2 promoters or engineered mutants lacking either the
361 AGTGCAAAG (mut1) or GGTTAAAAG (mut2) motifs. The results showed that TCF4
362 overexpression robustly activated the wt and mut2 promoters, but failed to enhance mut1-driven
363 luciferase activity, confirming that transcriptional activation depends critically on the
364 AGTGCAAAG site (Figure 3C). MDA-MB-468 and MDA-MB-231cells were subsequently

Accepted manuscript

365 transfected with si-NC or si-β-catenin, and it was observed that si-β-catenin transfection
366 significantly reduced β-catenin protein level in cells (Figure 3D). In addition, β-catenin knockdown
367 reduced the binding of TCF4 to the NEK2 promoter region (Figure 3E). In summary,
368 β-catenin/TCF4 mediated transcriptional activation of NEK2 in TNBC cells.

369 **TCF4 inhibited the sensitivity of TNBC cells to PTX through NEK2 regulation.** To dissect the
370 role of TCF4-mediated NEK2 regulation in TNBC chemoresistance, both TCF4 knockdown and
371 NEK2 overexpression were induced in TNBC cells. It was first observed that si-TCF4 transfection
372 significantly reduced NEK2 mRNA and protein levels in TNBC cells, while the con-transfection of
373 oe-NEK2 restored its expression (Figures 4A, 4B). Functional experiments showed that TCF4
374 knockdown further enhanced PTX-induced decrease in TNBC cell viability, while NEK2
375 overexpression partially rescued viability impaired by TCF4 silencing (Figure 4C). Additionally,
376 PTX-induced apoptosis in TNBC cells was further enhanced by TCF4 knockdown, while this
377 change was partially eliminated by NEK2 overexpression (Figure 4D). Furthermore, TCF4
378 silencing upregulated pro-apoptotic proteins Bax and cleaved caspase-3 in PTX-treated TNBC cells,
379 which was partially abolished by NEK2 overexpression (Figure 4E). In conclusion, TCF4
380 upregulation enhanced PTX resistance in TNBC cells by upregulating NEK2.

381 **M2-TAMs conferred PTX resistance in TNBC via the XCR1/β-catenin/TCF4/NEK2 axis.** To
382 investigate whether M2-TAMs promote chemoresistance through the β-catenin/TCF4/NEK2
383 cascade, si-NEK2-transfected MDA-MB-468 and MDA-MB-231 cells were treated with M2-CM
384 and PTX. The transfection efficiency was shown in Figures 5A and 5B, and the results
385 demonstrated that si-NEK2 transfection significantly reduced NEK2 expression in MDA-MB-468
386 and MDA-MB-231 cells. PTX decreased nuclear β-catenin and NEK2 expression in TNBC cells,
387 whereas M2-CM treatment partially reversed this inhibition (Figure 5C). Notably, NEK2 silencing
388 abolished M2-CM-induced NEK2 upregulation but had no significant effect on β-catenin nuclear
389 localization (Figure 5C). Functional assays demonstrated that M2-CM restored PTX-treated TNBC
390 cell viability, while this effect of M2-CM was partially attenuated by NEK2 knockdown in TNBC
391 cells (Figure 5D). Similarly, M2-CM suppressed PTX-induced apoptosis in TNBC cells, whereas
392 NEK2 silencing partially eliminated this change induced by M2-CM (Figure 5E). It also turned out
393 that M2-CM treatment reduced Bax and cleaved caspase-3 protein levels in PTX-treated TNBC

Accepted manuscript

394 cells, while NEK2 silencing partially abolished M2-CM-mediated suppression of these
395 pro-apoptotic markers (Figure 5F). To evaluate the translational relevance and therapeutic
396 specificity of the XCL2/XCR1/β-catenin/TCF4/NEK2 axis, we performed additional experiments
397 using the non-malignant human mammary epithelial cell line MCF-10A. Cells were treated with
398 PTX (50 nM) in the presence or absence of M2+si-NC-CM or M2+si-XCL2-CM. As shown in
399 Supplementary Figure **S1A**, PTX treatment significantly reduced MCF-10A cell viability, but
400 neither M2+si-NC-CM nor M2+si-XCL2-CM affected PTX-induced viability reduction.
401 Consistently, PTX treatment increased apoptosis in MCF-10A cells, while neither M2+si-NC-CM
402 nor M2+si-XCL2-CM significantly altered PTX-induced apoptosis (Supplementary Figure S1B).
403 Furthermore, PTX decreased nuclear β-catenin and NEK2 protein levels in MCF-10A cells,
404 whereas M2+si-NC-CM or M2+si-XCL2-CM did not significantly rescue these decreases
405 (Supplementary Figure S1C). All these results indicated that M2-TAMs enhanced PTX resistance in
406 TNBC by activating the β-catenin/TCF4/NEK2 signaling.
407 **M2-TAM-derived XCL2 was associated with attenuated PTX efficacy in TNBC *in vivo*.** To
408 validate the role of M2-TAM-secreted XCL2 in TNBC PTX resistance, we generated
409 THP-1-derived M2 macrophages with stable XCL2 knockdown and co-injected them with
410 MDA-MB-468 cells into nude mice, followed by PTX treatment. The knockdown efficiency of
411 XCL2 in THP-1 cells was shown in Figure 6A, and it was found that the infection of sh-XCL2
412 lentivirus significantly reduced XCL2 protein level in cells. It was subsequently observed that PTX
413 monotherapy suppressed tumor growth, whereas co-injection with M2 macrophages significantly
414 reversed this suppression (Figures 6B-6D). Strikingly, compared with sh-NC-M2 macrophages,
415 sh-XCL2-M2 macrophages treatment inhibit tumor progression (Figures 6B-6D).
416 Immunohistochemistry analysis revealed that PTX reduced Ki67 and NEK2 levels while increasing
417 Bax level in tumor tissues (Figure 6E). For negative controls, isotype-matched IgG was used instead
418 of primary antibodies, which showed no non-specific staining (Supplementary Figure S2). However,
419 M2 macrophage co-injection increased XCL2, NEK2, and Ki67 expression while reducing Bax,
420 with XCL2-deficient macrophages failing to induce similar effects (Figure 6E). Additionally, PTX
421 treatment significantly reduced nuclear β-catenin level in tumor tissues (Figure 6F). Importantly,
422 PTX-induced inhibition on nuclear β-catenin level was rescued by M2 macrophages but not by

Accepted manuscript

XCL2-deficient variants (Figure 6F). Collectively, M2-TAMs was associated with attenuated PTX efficacy in TNBC.

Discussion

TNBC is recognized as the most aggressive subtype of breast cancer, featured by a narrow spectrum of therapeutic options and dismal clinical prognosis due to intrinsic resistance to chemotherapy [21]. While PTX remains a cornerstone treatment, the development of chemoresistance severely compromises its efficacy [22]. Recent studies have highlighted M2-TAMs favor tumor development and play key roles in promoting chemoresistance [23]. However, the role of M2-TAMs in regulating PTX resistance during TNBC development remains unclear. Our study suggests a potential mechanism whereby M2-TAM-derived XCL2 may drive PTX resistance in TNBC. Specifically, M2-TAM-derived XCL2 was associated with inhibited PTX-driven cancer cell apoptosis and promoted PTX resistance in TNBC, potentially involving XCR1-mediated signaling through the β-catenin/TCF4/NEK2 axis (Figure 7).

XCL2 is a structurally conserved chemokine involved in the development and activation of cytotoxic T cells as well as the progression of malignant tumors [24, 25]. XCL2 expression exhibits a significant correlation with tumor-infiltrating immune cells in human cancers [9]. XCL2 is a key molecule in pan-cancer cells, and decreased XCL2 expression is associated with suppressed proliferation of breast cancer cells [26]. Importantly, our preliminary findings suggest that XCL2 may be a key gene influencing chemotherapy resistance in breast cancer [8]. Our current results displayed that XCL2 levels were significantly increased both intracellularly and in the CM upon M2 polarization of M0 macrophages. In addition, M2-CM treatment significantly reduced TNBC cell sensitivity to PTX *in vitro*, while CM derived from XCL2-knockdown M2 macrophages lost this ability. Our *in vivo* results demonstrated that M2-TAM-derived XCL2 was associated with attenuated PTX efficacy in TNBC, whereas XCL2 knockdown restored PTX efficacy. These data suggested that M2-TAMs promoted PTX resistance in TNBC by secreting XCL2.

The XCR1 receptor, the primary binding partner of XCL2, belongs to the chemokine receptor family and is known to activate various intracellular signaling cascades upon ligand binding [7]. The binding of C-chemokines to XCR1 promotes cancer cell proliferation [27-29]. Notably, XCR1

Accepted manuscript

452 activation is associated with TNBC development [10]. The binding of XCL1 to XCR1 promoted
453 epithelial–mesenchymal transition in breast cancer by enhancing β-catenin nuclear translocation
454 [10]. Activation of β-catenin promotes chemotherapy resistance in multiple cancer types [30, 31]. In
455 TNBC, the inhibition of β-catenin signaling suppresses cancer cell malignant behaviors [32]. In the
456 current research, PTX decreased nuclear β-catenin in TNBC cells, and M2-CM reinstated β-catenin
457 nuclear localization, but M2+si-XCL2-CM lost this ability. In addition, XCR1 knockdown in TNBC
458 cells reversed the M2-CM-mediated promotion of PTX resistance in TNBC. Collectively,
459 M2-TAM-derived XCL2 was associated with impaired PTX sensitivity in TNBC cells, potentially
460 via the XCR1/β-catenin axis.
461 β-catenin, upon nuclear translocation, forms complexes with transcription factors such as TCF4 to
462 regulate expression of target genes involved in cell proliferation and survival [33]. The
463 β-catenin/TCF4 complex has been implicated in various cancers enhancing chemotherapy
464 resistance in various cancers [34, 35]. Our work identified NEK2 as a novel transcriptional target of
465 β-catenin/TCF4 in TNBC. Numerous studies have reported NEK2 overexpression in various
466 cancers, where it is often associated with poor overall survival [36]. Additionally, NEK2 contributes
467 to drug resistance and cancer progression [37]. As previously reported, NEK2 knockdown inhibited
468 TNBC progression [38]. Our present findings demonstrated that TCF4 silencing sensitized TNBC
469 cells to PTX, which was abolished by NEK2 overexpression. Additionally, NEK2 knockdown in
470 TNBC cells reversed the M2-CM-mediated promotion of PTX resistance in TNBC. To further
471 evaluate the translational relevance of our findings, we examined whether the
472 XCL2/XCR1/β-catenin/TCF4/NEK2 axis functions similarly in non-malignant mammary epithelial
473 cells. Using the human mammary epithelial cell line MCF-10A, we found that neither
474 M2+si-NC-CM nor M2+si-XCL2-CM treatment protected normal breast epithelial cells from
475 PTX-induced cytotoxicity and regulated the downstream β-catenin/TCF4/NEK2 signaling. These
476 results suggest that therapeutic targeting of the XCL2/XCR1 axis or downstream effectors may
477 selectively sensitize TNBC cells to PTX while minimizing toxicity to normal breast tissue, thereby
478 providing a favorable therapeutic window for clinical translation. All these results indicated that
479 M2-TAM-derived XCL2 enhanced PTX resistance in TNBC by activating the
480 β-catenin/TCF4/NEK2 signaling.

Accepted manuscript

In summary, this study reveals that M2-TAM-derived XCL2 is associated with enhanced PTX resistance in TNBC, potentially through the XCR1/β-catenin/TCF4/NEK2 signaling axis. Mechanistically, XCL2 may bind to XCR1 and trigger β-catenin nuclear translocation, where it complexes with TCF4 to transcriptionally upregulate NEK2. Our findings suggest that targeting XCL2-XCR1 signaling or downstream effectors (β-catenin/NEK2) may restore PTX sensitivity in TNBC patients with high M2-TAM infiltration. However, limitations include the need for validation in larger clinical cohorts. Several limitations of the current study should be acknowledged. First, THP-1-derived macrophages were used as a model of TAMs. While this approach is widely employed in tumor microenvironment research due to its consistency, reproducibility, and ease of manipulation, THP-1 cells may not fully recapitulate the phenotypic and functional heterogeneity of primary TAMs isolated from patient breast tumors. Future validation using primary human monocyte-derived macrophages or freshly isolated TAMs from clinical specimens is warranted to confirm our findings. Second, the *in vivo* experiments were conducted using immunodeficient nude mice, which lack a functional immune system and thus cannot fully model the complex immune interactions within the tumor microenvironment. the therapeutic efficacy of XCL2/XCR1-targeted strategies (e.g., XCL2-neutralizing antibodies or XCR1 antagonists) in combination with PTX should be evaluated in patient-derived xenograft (PDX) models and genetically engineered mouse models of TNBC. Future studies should employ immunocompetent syngeneic mouse models or humanized immune system mice to better recapitulate the complex immune interactions within the tumor microenvironment and validate the therapeutic efficacy of XCL2/XCR1-targeted strategies in an immunologically intact setting.

Acknowledgement: This work was supported by Natural Science Foundation of Hunan Province (2024JJ9559).

Supplementary data are available in the online version of the paper.

References

Accepted manuscript

510 [1] SUN YS, ZHAO Z, YANG ZN, XU F, LU HJ et al. Risk Factors and Preventions of Breast
511 Cancer. Int J Biol Sci 2017; 13: 1387-1397. https://doi.org/10.7150/ijbs.21635
512 [2] CHEN Z, WU J, WANG L, ZHAO H, HE J. Tumor-associated macrophages of the M1/M2
513 phenotype are involved in the regulation of malignant biological behavior of breast cancer
514 cells through the EMT pathway. Med Oncol 2022; 39: 83.
515 https://doi.org/10.1007/s12032-022-01670-7
516 [3] LEON-FERRE RA, GOETZ MP. Advances in systemic therapies for triple negative breast
517 cancer. BMJ 2023; 381: e071674. https://doi.org/10.1136/bmj-2022-071674
518 [4] FERRARI P, SCATENA C, GHILLI M, BARGAGNA I, LORENZINI G et al. Molecular
519 Mechanisms, Biomarkers and Emerging Therapies for Chemotherapy Resistant TNBC. Int J
520 Mol Sci 2022; 23: 1665. https://doi.org/10.3390/ijms23031665
521 [5] DEEPAK KGK, VEMPATI R, NAGARAJU GP, DASARI VR, NAGINI S et al. Tumor
522 microenvironment: Challenges and opportunities in targeting metastasis of triple negative
523 breast cancer. Pharmacol Res 2020; 153: 104683. https://doi.org/10.1016/j.phrs.2020.104683
524 [6] DESWAL B, BAGCHI U, KAPOOR S. Curcumin Suppresses M2 Macrophage-derived
525 Paclitaxel Chemoresistance through Inhibition of PI3K-AKT/STAT3 Signaling. Anticancer
526 Agents Med Chem 2024; 24: 146-156.
527 https://doi.org/10.2174/0118715206275259231105184959
528 [7] NI LY, ZHOU L, WANG HQ, LUO XC, DAN XM et al. Identification and expression
529 analysis of three XCR1-like receptors from Epinephelus coioides after Cryptocaryon irritans
530 infection. Fish Shellfish Immunol 2017; 67: 95-102.
531 https://doi.org/10.1016/j.fsi.2017.06.010
532 [8] DENG Y, WANG J, HU Z, CAI Y, XU Y et al. Exploration of the immune
533 microenvironment of breast cancer in large population cohorts. Front Endocrinol (Lausanne)
534 2022; 13: 955630. https://doi.org/10.3389/fendo.2022.955630
535 [9] CHEN W, ZOU F, SONG T, XIA Y, XING J et al. Comprehensive analysis reveals XCL2 as
536 a cancer prognosis and immune infiltration-related biomarker. Aging (Albany NY) 2023; 15:
537 11891-11917. https://doi.org/10.18632/aging.205156
538 [10] DO HTT, CHO J. Involvement of the ERK/HIF-1α/EMT Pathway in XCL1-Induced
539 Migration of MDA-MB-231 and SK-BR-3 Breast Cancer Cells. Int J Mol Sci 2020; 22: 89.
540 https://doi.org/10.3390/ijms22010089
541 [11] GULATI R, HANLON MA, LUTZ M, QUITMEYER T, GELLER J et al.
542 Phosphorylation-Mediated Activation of β-Catenin-TCF4-CEGRs/ALCDs Pathway Is an
543 Essential Event in Development of Aggressive Hepatoblastoma. Cancers (Basel) 2022; 14:
544 6062. https://doi.org/10.3390/cancers14246062
545 [12] LIU Z, LIU H, DESAI S, SCHMITT DC, ZHOU M et al. miR-125b functions as a key
546 mediator for snail-induced stem cell propagation and chemoresistance. J Biol Chem 2013;
547 288: 4334-4345. https://doi.org/10.1074/jbc.M112.419168
548 [13] MARINA M, SAAVEDRA HI. Nek2 and Plk4: prognostic markers, drivers of breast
549 tumorigenesis and drug resistance. Front Biosci (Landmark Ed) 2014; 19: 352-365.
550 https://doi.org/10.2741/4212
551 [14] NARO C, DE MUSSO M, DELLE MONACHE F, PANZERI V, DE LA GRANGE P et al.
552 The oncogenic kinase NEK2 regulates an RBFOX2-dependent pro-mesenchymal splicing

Accepted manuscript

553 program in triple-negative breast cancer cells. J Exp Clin Cancer Res 2021; 40: 397.
554 https://doi.org/10.1186/s13046-021-02210-3
555 [15] NARO C, BARBAGALLO F, CAGGIANO C, DE MUSSO M, PANZERI V et al.
556 Functional Interaction Between the Oncogenic Kinase NEK2 and Sam68 Promotes a
557 Splicing Program Involved in Migration and Invasion in Triple-Negative Breast Cancer.
558 Front Oncol 2022; 12: 880654. https://doi.org/10.3389/fonc.2022.880654
559 [16] LEE J, GOLLAHON L. Nek2-targeted ASO or siRNA pretreatment enhances anticancer
560 drug sensitivity in triple- negative breast cancer cells. Int J Oncol 2013; 42: 839-847.
561 https://doi.org/10.3892/ijo.2013.1788
562 [17] ROBERTS MS, SAHNI JM, SCHROCK MS, PIEMONTE KM, WEBER-BONK KL et al.
563 LIN9 and NEK2 Are Core Regulators of Mitotic Fidelity That Can Be Therapeutically
564 Targeted to Overcome Taxane Resistance. Cancer Res 2020; 80: 1693-1706.
565 https://doi.org/10.1158/0008-5472.CAN-19-3466
566 [18] MODI K, LAWSON S, CHEN G, TUMULURI D, REKHTMAN I et al.
567 1-Chromonyl-5-Imidazolylpentadienone Demonstrates Anti-Cancer Action against TNBC
568 and Exhibits Synergism with Paclitaxel. Int J Mol Sci 2020; 21: 5777.
569 https://doi.org/10.3390/ijms21165777
570 [19] YANG B, LI G, WANG S, ZHENG Y, ZHANG J et al. Tumor-associated
571 macrophages/C-X-C motif chemokine ligand 1 promotes breast cancer autophagy-mediated
572 chemoresistance via IGF1R/STAT3/HMGB1 signaling. Cell Death Dis 2024; 15: 743.
573 https://doi.org/10.1038/s41419-024-07123-5
574 [20] WANG S, LI J, HONG S, WANG N, XU S et al. Chemotherapy-elicited extracellular vesicle
575 CXCL1 from dying cells promotes triple-negative breast cancer metastasis by activating
576 TAM/PD-L1 signaling. J Exp Clin Cancer Res 2024; 43: 121.
577 https://doi.org/10.1186/s13046-024-03050-7
578 [21] GIANNI L, HUANG CS, EGLE D, BERMEJO B, ZAMAGNI C et al. Pathologic complete
579 response (pCR) to neoadjuvant treatment with or without atezolizumab in triple-negative,
580 early high-risk and locally advanced breast cancer: NeoTRIP Michelangelo randomized
581 study. Ann Oncol 2022; 33: 534-543. https://doi.org/10.1016/j.annonc.2022.02.004
582 [22] LIAO L, ZHANG YL, DENG L, CHEN C, MA XY et al. Protein Phosphatase 1 Subunit
583 PPP1R14B Stabilizes STMN1 to Promote Progression and Paclitaxel Resistance in
584 Triple-Negative Breast Cancer. Cancer Res 2023; 83: 471-484.
585 https://doi.org/10.1158/0008-5472.CAN-22-2709
586 [23] LAN H, LIU Y, LIU J, WANG X, GUAN Z et al. Tumor-Associated Macrophages Promote
587 Oxaliplatin Resistance via METTL3-Mediated m(6)A of TRAF5 and Necroptosis in
588 Colorectal Cancer. Mol Pharm 2021; 18: 1026-1037.
589 https://doi.org/10.1021/acs.molpharmaceut.0c00961
590 [24] ZHOU B, XU H, NI K, NI X, SHEN J. Expression of Chemokine XCL2 and CX3CL1 in
591 Lung Cancer. Med Sci Monit 2016; 22: 1560-1565. https://doi.org/10.12659/msm.895985
592 [25] FERRY A, MEMPEL KM, MONELL A, REINA-CAMPOS M, SCHARPING NE et al. The
593 XCL1-XCR1 axis supports intestinal tissue residency and antitumor immunity. J Exp Med
594 2025; 222: e20240776. https://doi.org/10.1084/jem.20240776

Accepted manuscript

595 [26] ZIMMERMAN JW, PENNISON MJ, BREZOVICH I, YI N, YANG CT et al. Cancer cell
596 proliferation is inhibited by specific modulation frequencies. Br J Cancer 2012; 106:
597 307-313. https://doi.org/10.1038/bjc.2011.523
598 [27] KIM M, ROOPER L, XIE J, RAYAHIN J, BURDETTE JE et al. The lymphotactin receptor
599 is expressed in epithelial ovarian carcinoma and contributes to cell migration and
600 proliferation. Mol Cancer Res 2012; 10:1419-1429.
601 https://doi.org/10.1158/1541-7786.MCR-12-0361
602 [28] WANG T, HAN S, WU Z, HAN Z, YAN W et al. XCR1 promotes cell growth and migration
603 and is correlated with bone metastasis in non-small cell lung cancer. Biochem Biophys Res
604 Commun 2015; 464: 635-641. https://doi.org/10.1016/j.bbrc.2015.06.175
605 [29] KHURRAM SA, WHAWELL SA, BINGLE L, MURDOCH C, MCCABE BM et al.
606 Functional expression of the chemokine receptor XCR1 on oral epithelial cells. J Pathol
607 2010; 221: 153-163. https://doi.org/10.1002/path.2695
608 [30] DONG S, LIANG S, CHENG Z, ZHANG X, LUO L et al. ROS/PI3K/Akt and
609 Wnt/β-catenin signalings activate HIF-1α-induced metabolic reprogramming to impart
610 5-fluorouracil resistance in colorectal cancer. J Exp Clin Cancer Res 2022; 41: 15.
611 https://doi.org/10.1186/s13046-021-02229-6
612 [31] WANG J, YU H, DONG W, ZHANG C, HU M et al. N6-Methyladenosine-Mediated
613 Up-Regulation of FZD10 Regulates Liver Cancer Stem Cells' Properties and Lenvatinib
614 Resistance Through WNT/β-Catenin and Hippo Signaling Pathways. Gastroenterology
615 2023; 164: 990-1005. https://doi.org/10.1053/j.gastro.2023.01.041
616 [32] ARZI L, MOLLAEI H, HOSHYAR R. Countering Triple Negative Breast Cancer via
617 Impeding Wnt/β-Catenin Signaling, a Phytotherapeutic Approach. Plants (Basel) 2022; 11:
618 2191. https://doi.org/10.3390/plants11172191
619 [33] MA X, HAN X, WANG W, ZHANG Q, TANG H. β-Catenin regulates ovarian granulosa
620 cell cycle and proliferation in laying hens by interacting with TCF4. Poult Sci 2024; 103:
621 103377. https://doi.org/10.1016/j.psj.2023.103377
622 [34] WANG JM, ZHANG FH, XIE HY, LIU ZX, TANG YJ et al. KIF26B promotes bladder
623 cancer progression via activating Wnt/β-catenin signaling in a TRAF2-dependent pathway.
624 Cell Rep 2025; 44: 115595. https://doi.org/10.1016/j.celrep.2025.115595
625 [35] LEE GT, ROSENFELD JA, KIM WT, KWON YS, PALAPATTU G et al. TCF4 induces
626 enzalutamide resistance via neuroendocrine differentiation in prostate cancer. PLoS One
627 2019; 14: e0213488. https://doi.org/10.1371/journal.pone.0213488
628 [36] XIA J, ZHAO H, EDMONDSON JL, KOSS B, ZHAN F. Role of NEK2 in tumorigenesis
629 and tumor progression. Trends Mol Med 2025; 31: 79-93.
630 https://doi.org/10.1016/j.molmed.2024.07.013
631 [37] FANG Y, ZHANG X. Targeting NEK2 as a promising therapeutic approach for cancer
632 treatment. Cell Cycle 2016; 15: 895-907. https://doi.org/10.1080/15384101.2016.1152430
633 [38] RIVERA-RIVERA Y, MARINA M, JUSINO S, LEE M, VELÁZQUEZ JV et al. The Nek2
634 centrosome-mitotic kinase contributes to the mesenchymal state, cell invasion, and
635 migration of triple-negative breast cancer cells. Sci Rep 2021; 11: 9016.
636 https://doi.org/10.1038/s41598-021-88512-0
637

Accepted manuscript

638

639 **Figure Legends**

640

641 **Figure 1.** M2-TAMs inhibited the sensitivity of TNBC cells to PTX by secreting XCL2. THP-1
642 cells were treated with PMA to induce M0 macrophages and further stimulated with IL-4+IL-13 for
643 M2 polarization. A) Flow cytometry was performed to detect M2 macrophage polarization markers
644 (CD206 and CD163). B, C) The mRNA and protein levels of XCL2 were determined using
645 RT-qPCR and Western blot. D) Secreted XCL2 in M0 and M2 macrophages was quantified by
646 ELISA. Note: Values represent original concentrations after correction for a 2-fold sample dilution,
647 as preliminary testing indicated that M2 supernatant XCL2 levels exceeded the assay upper limit
648 (480 ng/ml). Values represent original concentrations after correction for a 2-fold dilution factor. E,
649 F) M2 macrophages were transfected with si-NC or si-XCL2, and the mRNA and protein levels of
650 XCL2 in cells were determined using RT-qPCR and Western blot. G) CM were collected from M0-,
651 M2-, M2+si-NC-, and M2+si-XCL2-treated macrophages, and XCL2 levels were measured by
652 ELISA. H) MDA-MB-468 and MDA-MB-231 cells were cultured with various PTX concentrations
653 (0-50 nM) plus different CM treatments, and cell viability was assessed by CCK-8 assay.
654 MDA-MB-468 and MDA-MB-231 cells were treated with PTX combined with different CM groups
655 (M0-CM, M2-CM, M2+si-NC-CM, and M2+si-XCL2-CM). I) CCK-8 assay was employed to
656 detect cell viability. J) Flow cytometry was employed to determine apoptosis in TNBC cells. K)
657 Bax and cleaved caspase-3 protein levels in TNBC cells were analyzed using Western blot. Data
658 were expressed as mean±SD. All our data were obtained from three independent experiments.
659 Student's t-test (two-tailed) for two-group comparisons (A-F), one-way ANOVA with Tukey's post
660 hoc test for multiple group comparisons (G, I-K), and two-way ANOVA followed by Sidak's post
661 hoc test was used to compare group differences at each time point (H). *$p < 0.05$, **$p < 0.01$, ***p
662 < 0.001

663

664 **Figure 2.** M2-TAM-derived XCL2 was associated with reduced PTX sensitivity in TNBC cells via
665 the XCR1/β-catenin axis. A) MDA-MB-468 and MDA-MB-231 cells were treated with PTX alone
666 or PTX+CM (M0, M2, M2+si-NC, M2+si-XCL2), and cytosolic and nuclear fractions were
667 analyzed by Western blot for β-catenin levels. MDA-MB-468 and MDA-MB-231 cells were

Accepted manuscript

668 transfected with si-NC or si-XCR1. B) RT-qPCR was performed to detect XCR1 mRNA level in
669 TNBC cells. C) Western blot was employed to detect XCR1 and nuclear β-catenin protein levels.
670 si-NC/si-XCR1 transfected MDA-MB-468 and MDA-MB-231 cells were treated with PTX
671 combined with M2-CM treatment. D) CCK-8 assay was employed to detect cell viability. E) Flow
672 cytometry was employed to determine apoptosis in TNBC cells. F) Bax and cleaved caspase-3
673 protein levels in TNBC cells were analyzed using Western blot. Data were expressed as mean±SD.
674 All our data were obtained from three independent experiments. Student's t-test (two-tailed) for
675 two-group comparisons (B, C), one-way ANOVA with Tukey's post hoc test for multiple group
676 comparisons (D-F). *$p < 0.05$, **$p < 0.01$, ***$p < 0.001$
677
678 **Figure 3.** TCF4 transcriptionally activated NEK2 expression in TNBC cells. A) The potential
679 binding sites between TCF4 and the NEK2 promoter were predicted using the JASPAR database. B)
680 ChIP-qPCR assay was employed to detect the interaction between TCF4 and the NEK2 promoter. C)
681 The transcriptional regulation relationship of TCF4 on NEK2 in 293T cells was analyzed by
682 dual-luciferase reporter assay. MDA-MB-468 and MDA-MB-231 cells were transfected with si-NC
683 or si-β-catenin. D) Western blot was performed to detect β-catenin protein level in TNBC cells. E)
684 The interaction between TCF4 and the NEK2 promoter was analyzed using ChIP-qPCR assay. Data
685 were expressed as mean±SD. All our data were obtained from three independent experiments.
686 Student's t-test (two-tailed) for two-group comparisons. **$p < 0.01$, ***$p < 0.001$
687
688 **Figure 4.** TCF4 inhibited the sensitivity of TNBC cells to PTX through NEK2 regulation. A-B)
689 MDA-MB-468 and MDA-MB-231 cells were co-transfected with si-TCF4 and oe-NEK2, and the
690 mRNA and protein levels of TCF4 and NEK2 were assessed using RT-qPCR and Western blot. Both
691 TCF4 knockdown and NEK2 overexpression were induced in MDA-MB-468 and MDA-MB-231
692 cells combined with PTX treatment. C) Cell viability was determined using CCK-8 assay. D) Flow
693 cytometry was employed to determine apoptosis in TNBC cells. E) Western blot was employed to
694 assess Bax and cleaved caspase-3 protein levels in TNBC cells. Data were expressed as mean±SD.
695 All our data were obtained from three independent experiments. One-way ANOVA with Tukey's
696 post hoc test for multiple group comparisons. *$p < 0.05$, **$p < 0.01$, ***$p < 0.001$

Accepted manuscript

697

698 **Figure 5.** M2-TAMs conferred PTX resistance in TNBC via the XCR1/β-catenin/TCF4/NEK2 axis.
699 A, B) MDA-MB-468 and MDA-MB-231 cells were transfected with si-NC or si-NEK2, and the
700 mRNA and protein levels of NEK2 in cells were assessed using RT-qPCR and Western blot.
701 si-NC/si-NEK2 transfected MDA-MB-468 and MDA-MB-231 cells were treated with PTX
702 combined with M2-CM treatment. C) Western blot was performed to detect NEK2 and nuclear
703 β-catenin protein levels in TNBC cells. D) CCK-8 assay was performed to determine cell viability.
704 E) Apoptosis in TNBC cells was assessed by flow cytometry. F) Bax and cleaved caspase-3 protein
705 levels in TNBC cells were analyzed using Western blot. Data were expressed as mean±SD. All our
706 data were obtained from three independent experiments. Student's t-test (two-tailed) for two-group
707 comparisons (A, B), one-way ANOVA with Tukey's post hoc test for multiple group comparisons
708 (C-F). *$p < 0.05$, **$p < 0.01$, ***$p < 0.001$

709

710 **Figure 6.** M2-TAM-derived XCL2 was associated with attenuated PTX efficacy in TNBC *in vivo*.
711 A) THP-1 were infected with sh-NC or sh-XCL2 lentivirus, and XCL2 protein level in cells was
712 determined using Western blot. THP-1-derived M2 macrophages with stable XCL2 knockdown and
713 co-injected them with MDA-MB-468 cells into nude mice, followed by PTX treatment. B) Tumor
714 growth curves (measured every 3 days from day 7) were presented. C, D) Representative tumor
715 images at endpoint were presented, and tumor weights were measured. E) Immunohistochemistry
716 was performed to detect XCL2, NEK2, Bax, and Ki67 protein levels in tumor tissues. Scale bar=50
717 μm. F) Nuclear β-catenin protein level was assessed using Western blot. Data were expressed as
718 mean±SD; n=6. One-way ANOVA with Tukey's post hoc test for multiple group comparisons (A,
719 C-F) and two-way ANOVA followed by Sidak's post hoc test was used to compare group
720 differences at each time point (B). *$p < 0.05$, **$p < 0.01$, ***$p < 0.001$

721

722 **Figure 7.** Graphical abstract. M2-TAM-derived XCL2 is associated with enhanced PTX resistance
723 in TNBC. Mechanistically, XCL2 may bind to XCR1 and trigger β-catenin nuclear translocation,
724 where it complexes with TCF4 to transcriptionally upregulate NEK2.

Accepted manuscript

Fig. 1 Download full resolution image

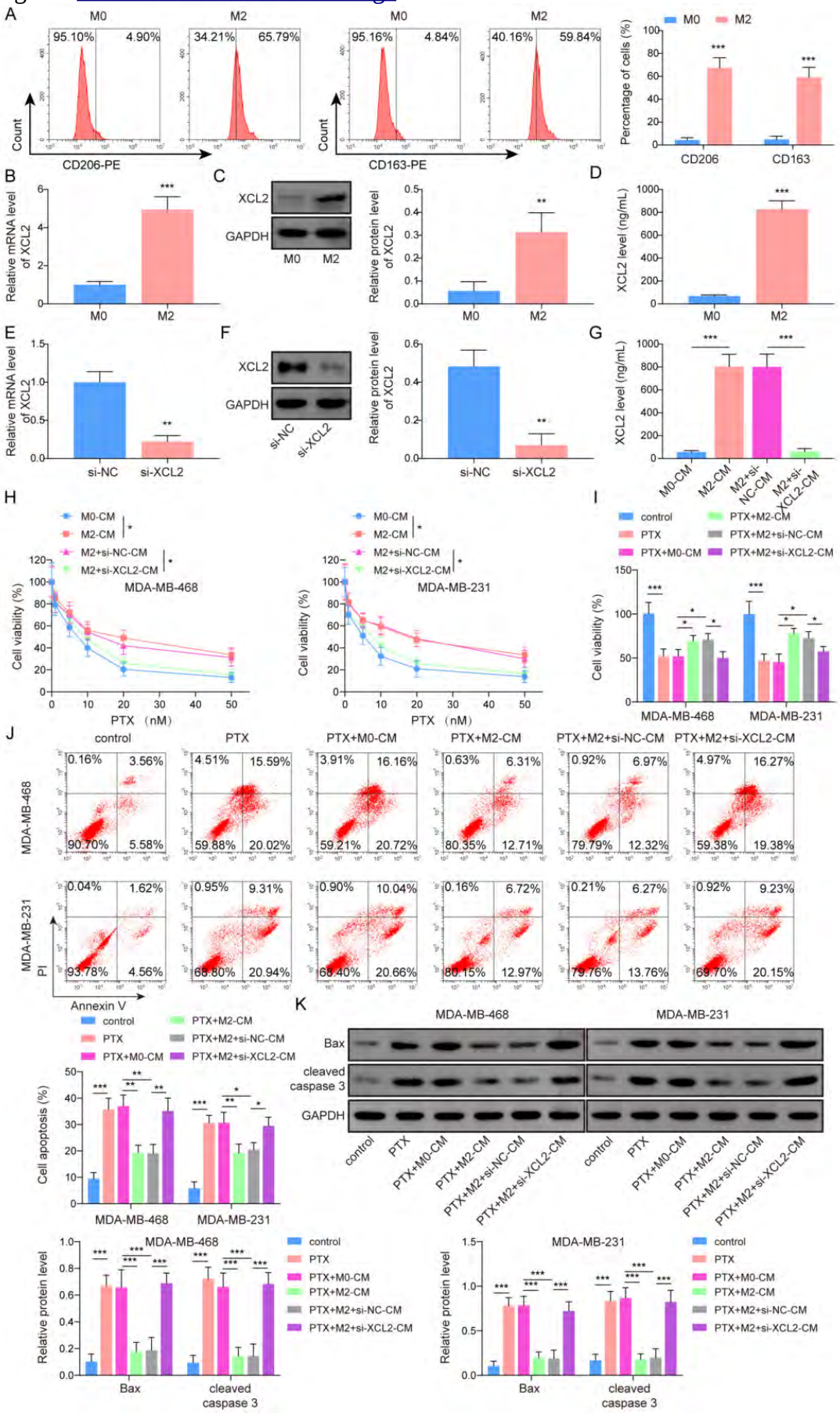

Fig. 2 Download full resolution image

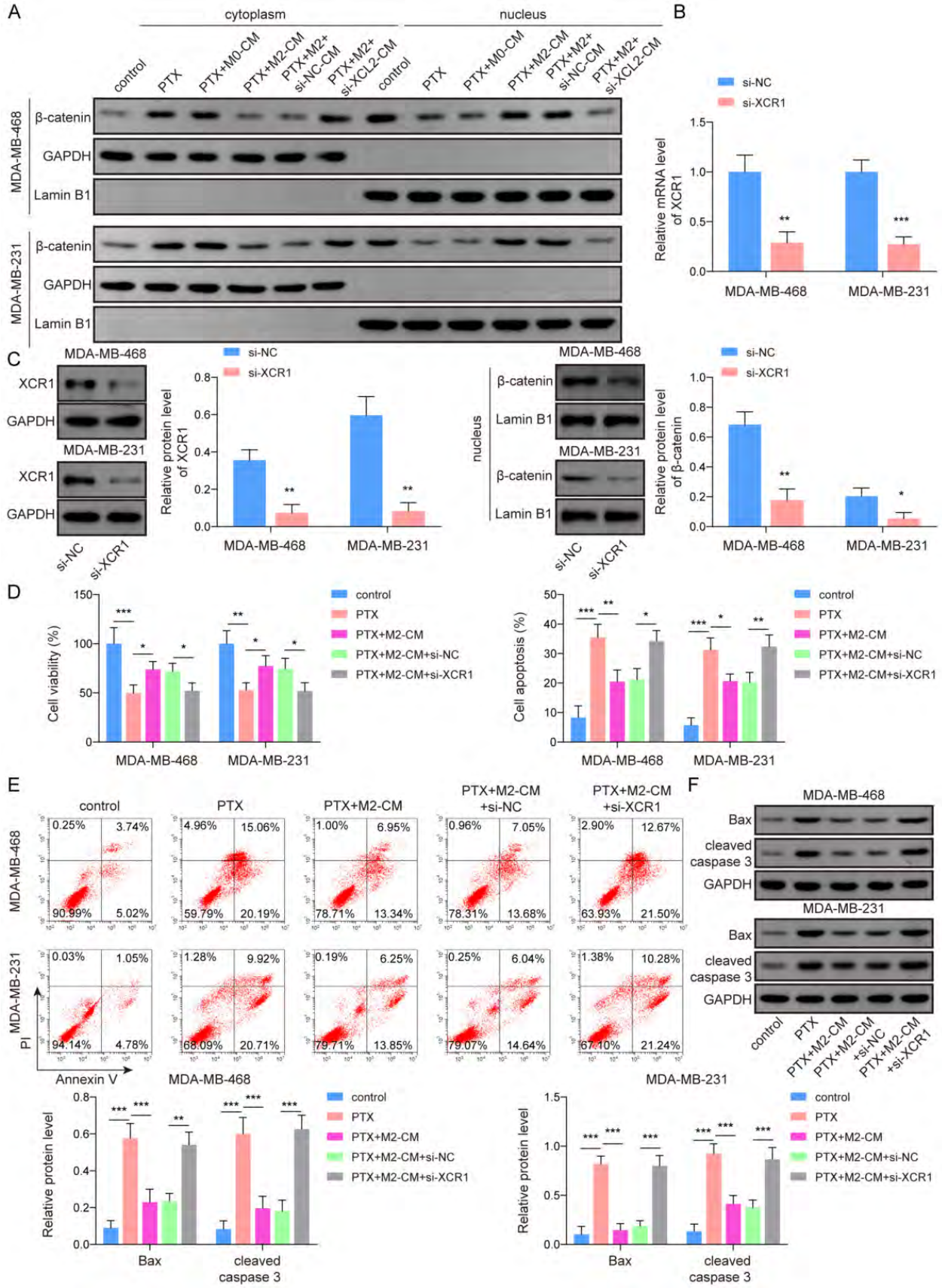

Fig. 3 Download full resolution image

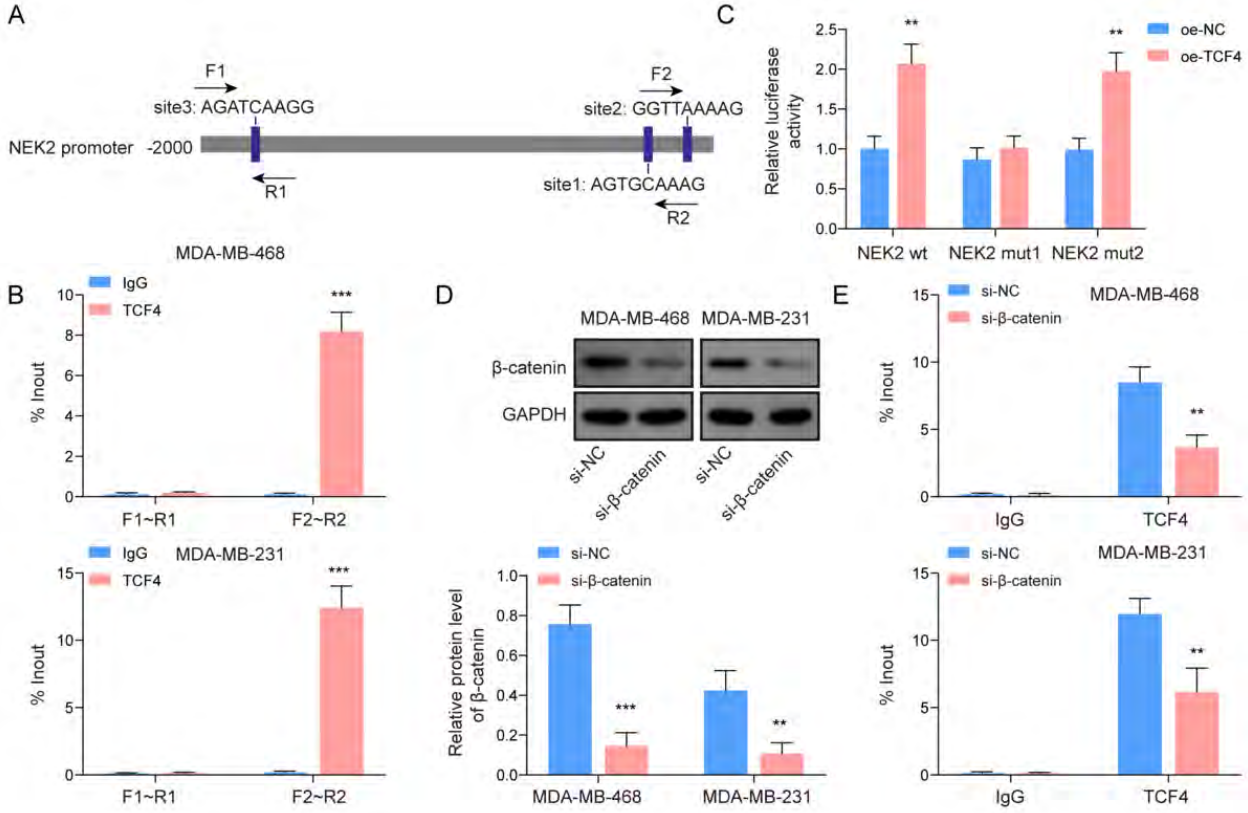

Fig. 4 Download full resolution image

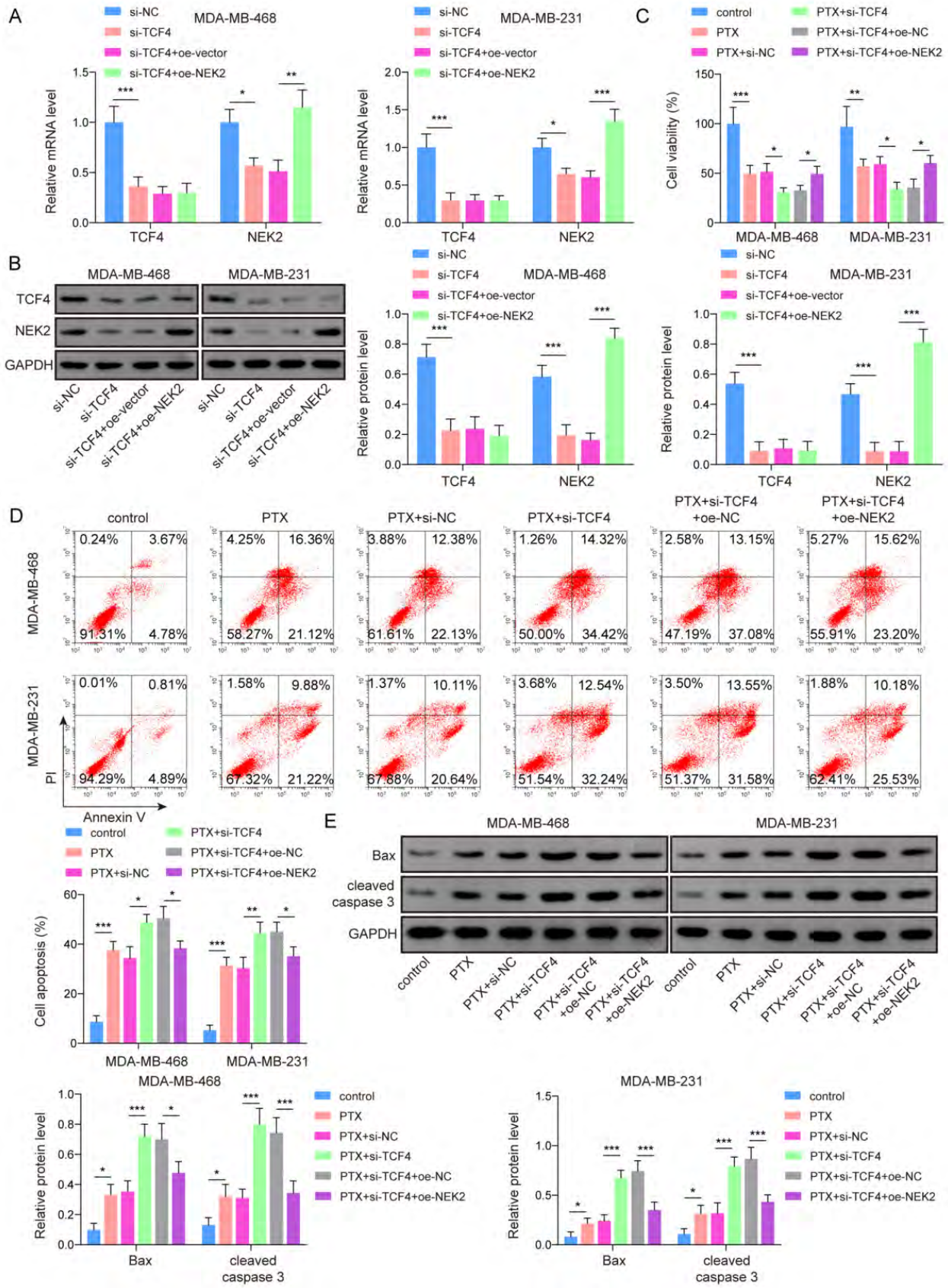

Fig. 5 Download full resolution image

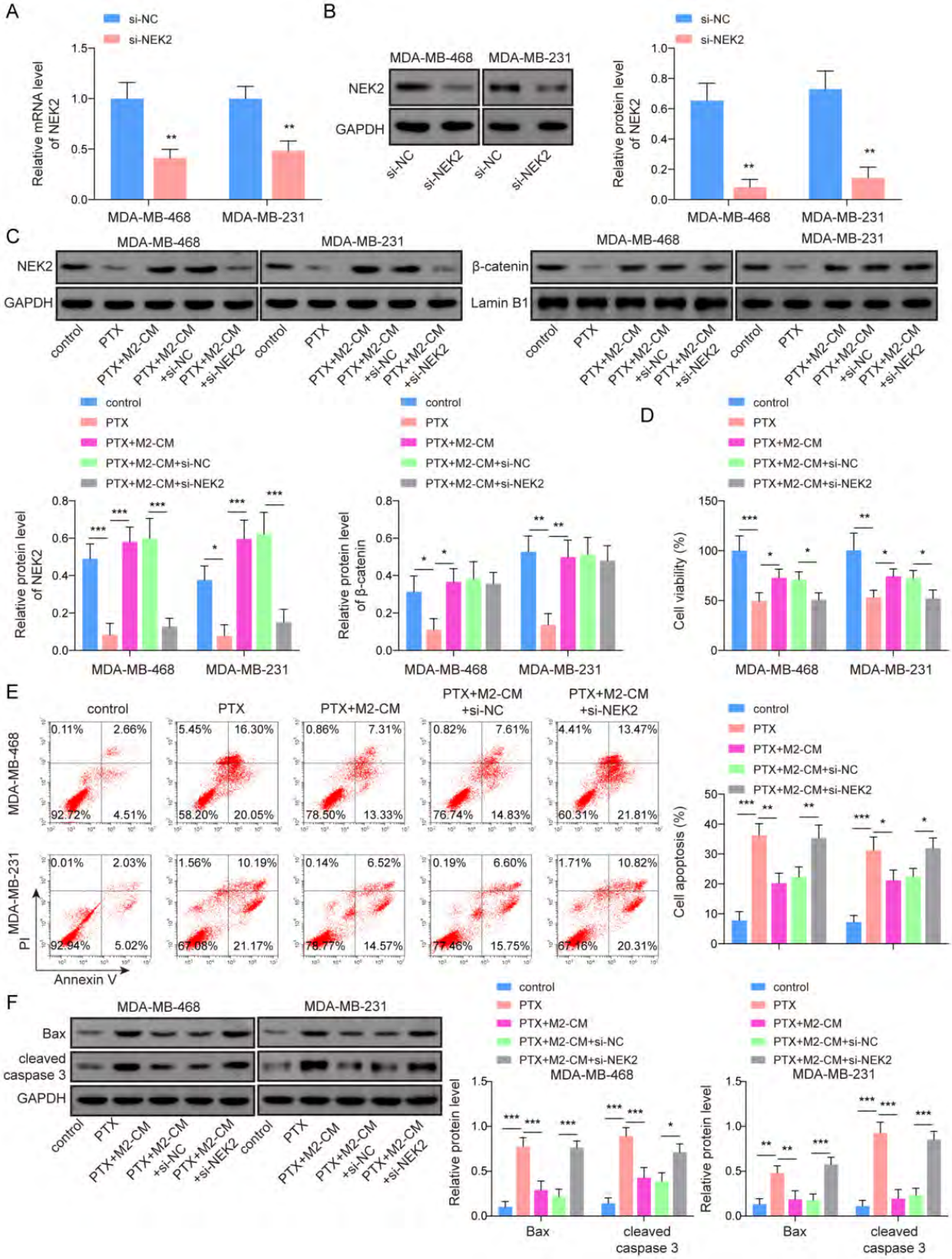

Fig. 6 Download full resolution image

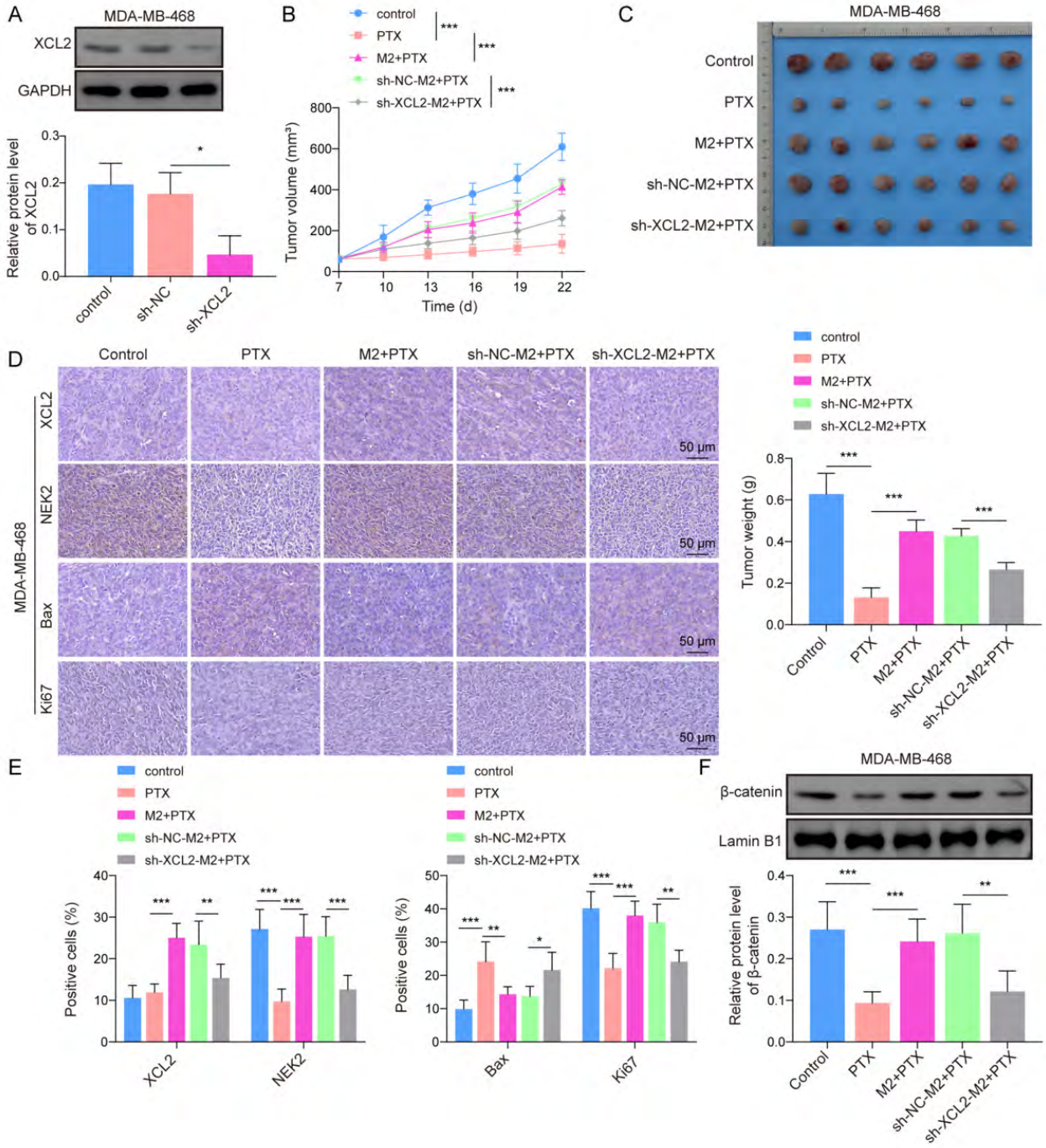
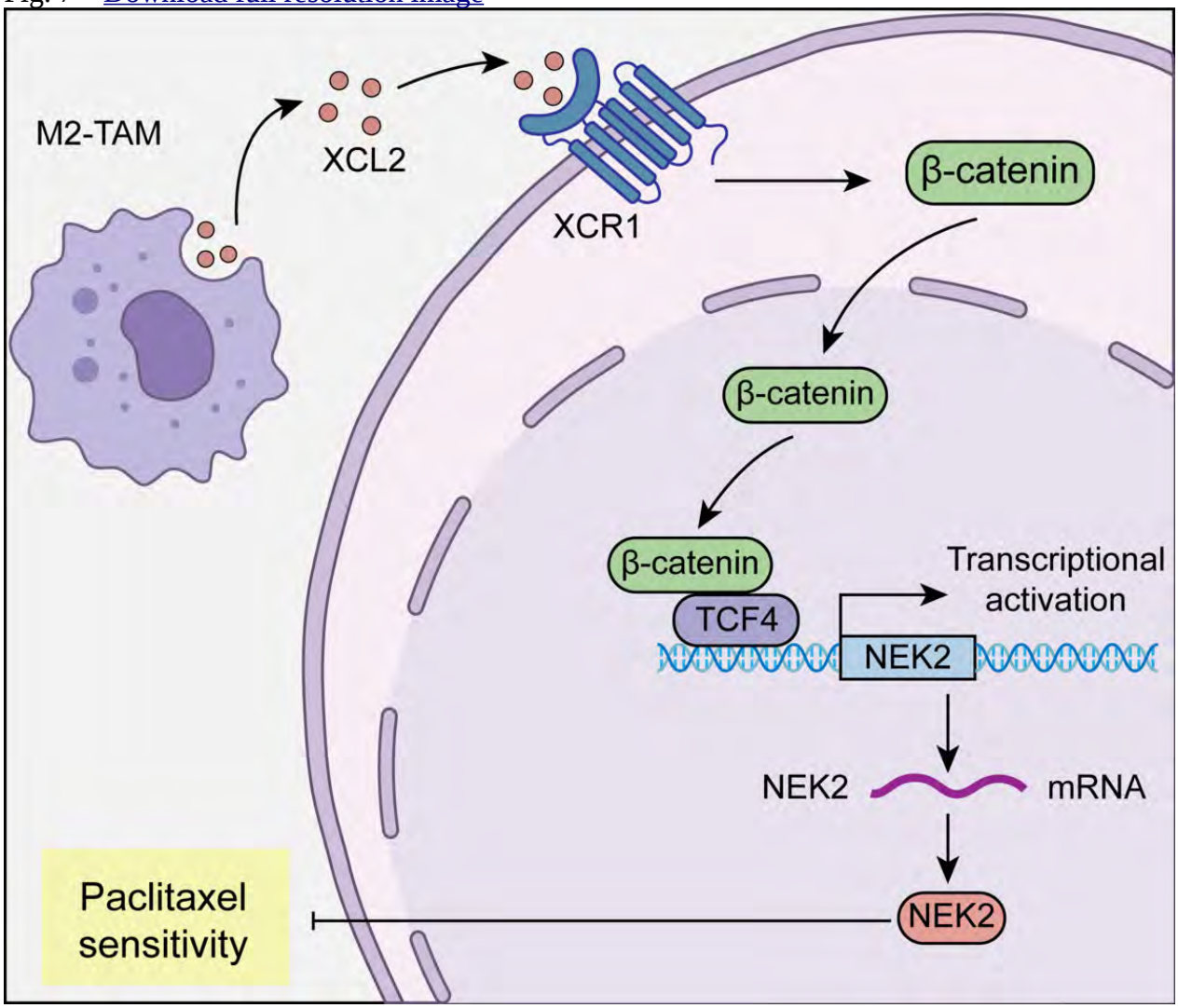
Fig. 7 Download full resolution image